Functional Connectivity Density Alterations in Children with Strabismus and Amblyopia based on Resting-state Functional Magnetic Resonance Imaging (fMRI)

Yi-Dan Shi
First Affiliated Hospital of Nanchang University
Qian-Min Ge
First Affiliated Hospital of Nanchang University
Qi Lin
First Affiliated Hospital of Nanchang University
Rong-Bin Liang
First Affiliated Hospital of Nanchang University
Qiu-Yu Li
First Affiliated Hospital of Nanchang University
Wen-Qing Shi
First Affiliated Hospital of Nanchang University
Biao Li
First Affiliated Hospital of Nanchang University
Yi Shao (freebee99@163.com)
First Affiliated Hospital of Nanchang University

Research Article

Keywords: strabismus, amblyopia, magnetic resonance imaging

Posted Date: August 18th, 2021

DOI: https://doi.org/10.21203/rs.3.rs-753249/v1

Version of Record: A version of this preprint was published at BMC Ophthalmology on February 2nd, 2022. See the published version at https://doi.org/10.1186/s12886-021-02228-3.

Abstract

Purpose: To investigate functional connectivity density (FCD) values of brain areas in children with strabismus and amblyopia (SA) by resting-state functional magnetic resonance imaging (rs-fMRI).

Methods: This study recruited 26 children (14 male, 12 female) with SA and 26 healthy children (14 male, 12 female) as healthy controls. Both groups matched in age, gender, educational level and socioeconomic background. All participants underwent fMRI scanning while resting. Visual function of participants was also evaluated by an ophthalmic examination; rs-fMRI data was then used to determine global and short-range FCD. Receiver operating characteristic curves were constructed to investigate whether there was a significant difference between children with SA and healthy controls. This experiment has passed the ethical approval and obtained the logic number cdyfy201511.

Results: Global FCD values of children with SA were found to be remarkably decreased in the right cerebellum, left lenticular nucleus, putamen, and right superior frontal gyrus as compared with healthy controls; global FCD values of children with SA were increased in the right angular gyrus, left middle cingulate gyrus, left angular gyrus, right superior parietal gyrus, and right middle frontal gyrus. In children with SA, short-range FCD values were found to be remarkably decreased in regions of the middle right temporal pole, right cerebellum, left lenticular nucleus, putamen, left hippocampus, right hippocampus, left thalamus, left cerebellum; values were increased in the right superior parietal gyrus as compared with healthy controls.

Conclusion: We noted abnormal neural connectivity in some brain areas of children with SA; the detailing of such connectivity aberrations is helpful in exploring the pathophysiology of SA and providing useful information for future clinical management.

Introduction

Both strabismus and amblyopia (SA) are widespread ophthalmologic conditions which frequently manifest in infancy. Extraocular muscle (EOM) dysfunction is believed to be among the primary etiologies of this condition, as is dysplasia, malnutrition and abnormal anatomy[1, 2]. Such pathology associates with maldevelopment of visual pathways responsible for the mediation of eye movement. If no timely and effective treatment is provided, symptoms persist into adulthood[3, 4]. Patients suffering strabismus cannot attain synchronized binocular vision as the visual axis of each eye remains in a state of misalignment with that of the contralateral eye. Such symptoms, in turn, lead to impairment of visual acuity. Common complications included amblyopia and stereoblindness. Strabismus frequently causes amblyopia, while amblyopia likewise results in perceptual strabismus without effective intervention.

The incidence of SA is thought to have increased as the development of society. The incidences of strabismus and amblyopia in eastern, and the whole of China, are 5.65% and 1%-3%, respectively[5, 6].

Strabismus not only affects vision in childhood, but also threatens psychological health, social functioning and early character formation[7–9].

Magnetic resonance imaging (MRI) is a noninvasive technique capable of delineating the anatomical structure and functional alterations of the brain [10]. Resting-state functional MRI (rs-fMRI) in particular produces high-resolution images which can accurately detail different functional brain regions simultaneously. Tremendous contributions to the research of many ophthalmic diseases have been made using rs-fMRI, including primary angle-closure glaucoma and corneal ulcers[11, 12]. Blood oxygen level-dependent (BOLD) fMRI is also frequently applied in clinical and scientific settings; local alterations in the neuronal hemodynamic response reveal neuronal spontaneous activity.

Functional connectivity reflects natural fluctuations in brain activity. Study of spontaneous brain functional activity via analysis of resting-state functional connectivity (rsFC) effectively details the temporal correlation of BOLD signals from different areas of the brain when imaged in succession[13].

Functional connectivity density (FCD) mapping, which includes both global (gFCD) and short-range (or local; lFCD) mapping, represents functional data of the entire brain using voxel-based morphometry. Greater gFCD values of certain functional areas suggest heightened levels of local activity and hence interneuronal communication [14]. Neuronal apoptosis, development, remodeling, and degeneration all result in changes in FCD, which has previously been used in research studying Parkinson's disease[15], Alzheimer's disease[16], and depression[17].

Prior studies reported that patients suffering amblyopia also suffered damage to multiple functional brain areas, as evidenced by white matter structure and gray matter morphology aberrations [18]. Lesions were not only observed in the visual cortex as well as the dorsal and ventral visual pathways, but also in higher-level brain areas vital to visual attention and cognition; alterations in functional connectivity among several brain areas instead of isolated, distinctly localized changes were thus found to be hallmark[19]. Here, we calculated gFCD and lFCD values based on rs-fMRI data, thereby exploring changes in spontaneous brain functional activity of children suffering SA.

1 Subjects And Methods

1.1 Subjects

The SA group consisted of 26 children who had sought medical care at the Eye Clinic of The First Affiliated Hospital of Nanchang University (Nanchang, China) and included 14 males and 12 females. Inclusion criteria were as follows: 1) children <18 years of age; 2) children diagnosed with strabismus; 3) children possessing a difference of >2 lines (≥0.20 logMAR units) between the best-corrected visual acuity of the amblyopic eye and uncorrected acuity in the unaffected eye as measured with subject view fixed straight ahead. Exclusion criteria were as follows: 1) a history of ocular surgery; 2) a history of other ophthalmologic conditions; 3) the presence of conditions precluding rs-fMRI imaging, including mental

conditions; 4) drug or alcohol addiction. A total of 26 healthy children who matched study subjects in age, sex, educational level and socioeconomic backgrounds were recruited into a healthy control (HC) group. Criteria for HC group recruitment were a lack of MRI findings attributable to cerebral parenchymal pathology, no history of ophthalmologic illness and no history of mental conditions (e.g. depressive psychosis, epilepsy). The visual acuity of all subjects was evaluated by Snellen chart. Subjects were examined with the horizontal distance between them and the vision chart maintained at 5 meters; their line of sight remained fixed parallel to the 1.0 mark on the chart. This study was approved by the Medical Ethics Committee of the First Affiliated Hospital of Nanchang University and written, informed consent was provided by all participants. This study was conducted in accordance with the Helsinki declaration.

1.2 MRI scanning

A Trio 3.0T MRI machine (Siemens, Germany) was used in this study and 8-channel head coils were used to obtain MRI images of the head; rs-fMRI data was acquired by echo planar imaging (EPI) sequence with the following parameters: TR/TE=2000ms/30ms; flip angle (FA)=90°; thickness=4mm; gap=1mm; layers=33; matrix=64×64; field of view (FOV)=240mm×240mm; containing 240 time points. High resolution structural phase data was acquired using the T1WI 3D MP-RAGE sequence with the following parameters: TR/TE =1900ms/2.26ms; FA=9°; thickness=1mm; gap=0mm; layers=156; matrix=256×256, FOV=240×240mm; scanning time=3 min. During MRI scanning, subjects were instructed to lie still and avoid movement as best as possible while keeping eyes closed, staying conscious and remaining relaxed. Subjects were instructed not to think of anything in particular during imaging.

1.3 Calculations

MRIcro software (www.MRIcro.com) was used to ensure high-quality data organization. The first 10 images were discarded to allow for equilibration and subject adaptation. The brain imaging data processing and analysis toolbox (DPABI 2.1, MathWorks ABI) based on MATLAB 2010a (MathWorks, http://rfmri.org/DP, USA) was adopted to precondition remaining data. All subjects remained still until scanning was completed. With reference to the Friston 24-parameter model, multiple linear regression analysis (6 head motion parameters, 6 head motion parameters from the previous time point, and 12 corresponding square items) was used to correct head movement and avoid issues such as inaccurate positioning due to head movement. Extraneous variables were subsequently eliminated using linear regression modeling. The Montreal Neurological Institute standard template was used as a reference image for spatial normalization when correcting for head motion. All voxel time series were band-pass filtered (0.01~0.08Hz) and data attenuated for both maximal accuracy and minimization of interference factors (e.g. heartbeat, respiratory noise).

1.4 Functional connectivity mapping

Both gFCD and lFCD maps were constructed. For gFCD values, this study used the method described by Tomasi and Volkow[13] to calculate values using an internal script. The Pearson linear correlation was applied and the correlation coefficient threshold was R> 0.6[13]. Only gray matter gFCD values were calculated (SNR> 50%) to ensure data accuracy. Finally, a 6×6×6mm^3 Gaussian kernel was used to spatially smooth the normalized gFCD map and reduce differences in data due to subject variations.

This study defined two diverse brain functional regions with an anatomical distance ≤14mm and correlation coefficient threshold (R) > 0.25 as a neighborhood with correlating activity; FCD maps were used to evaluate subject gray matter (GM). Based on the Pearson correlation coefficient, the number of functional connections of a prescribed voxel was regarded as the degree of nodes in the binary graph. The BrainWave toolbox (http://cran.rproject.org/src/conTRIB/Archive/Brainwaver) was used to calculate lFCD values. First, global functional connectivity between a given voxel and other voxels was defined by a correlation threshold r> 0.25. Then, lFCD and gFCD values were converted into Z points. Statistical parameters were finally utilized for mapping in SPM8 (MathWorks, USA) and a 6×6×6mm^3 Gaussian kernel was used to spatially smooth the normalized gFCD map.

1.5 Correlation analyses

This study used SPSS 20.0 software (SPSS, USA) to evaluate the relationship between abnormal brain functional areas in children suffering SA and anxiety or depression. This study used the Hospital Anxiety and Depression Scale (HADS) to evaluate the levels of anxiety and depression experienced by our subjects[20]. Participants were inquired as to their psychological status over the prior month. The maximum score for anxiety and/or depression was 21; scores of 0~7 implied no symptoms; scores of 8~10 implied possible symptoms; scores of 11~21 implied certain symptoms. Patients were considered as anxious or depressed when scores ≥8 were noted.

1.6 Statistical analyses

Differences among SA and HC groups were analyzed using SPSS 20.0 software (SPSS, USA) and the independent t-test (P <0.05). Here, we detected discrepancies of gFCD and lFCD averages among SA and HC group subjects using SPM8 software (MathWorks, USA) by applying a general linear model and the double sample t-test. Age and gender were used as correlates in the evaluation of cerebral blood flow graph differences among SA patients and HC subjects; GRF correction was used as the significance criterion for data correction (voxel level P <0.01, cluster level P <0.05). Moreover, receiver operating characteristic (ROC) curve construction and Pearson correlation analysis were both applied to estimate gFCD and lFCD values of two given functional areas as well as the relationship between mean gFCD and lFCD of these areas.

2 Results

2.1 Subject data

No significant differences among SA and HC subjects were noted in age (P=0.884); best-corrected left eye (P=0.012) and right eye (P=0.007) acuity significantly differed *(table 1).*

Table 1

Participant characteristics

Condition	SA	HCs	t	P-value*
Male/female	14/12	14/12	N/A	>0.999
Age (years)	8.21±2.12	8.38±1.86	0.259	0.884
Weight (kg)	20.58±2.98	21.03±3.74	0.462	0.817
Handedness	26R	26R	N/A	N/A
Duration of SA (years)	7.01±2.32	N/A	N/A	N/A
BCVA-left eye	0.20±0.05	1.00±0.15	−3.158	0.012
BCVA-right eye	0.50±0.15	1.10±0.10	−3.653	0.007
IOP-L	14.65±4.16	15.12±4.03	0.696	0.853
IOP-R	13.46±3.27	14.53±4.11	0.721	0.834

Notes: Independent t-tests comparing the two groups ($p<0.05$ represented statistically significant differences). Data shown as mean standard deviation or n.

Abbreviations: BCVA, best-corrected visual acuity; HCs, healthy controls; IOP, intraocular pressure; L, left; N/A, not applicable; R, right□SA, strabismus and amblyopia

2.2 Functional connectivity density analysis

As compared to HC subjects, gFCD values of SA patients were markedly decreased in the right cerebellum, left lenticular nucleus, left putamen and right superior frontal gyrus; gFCD values were increased in the right angular gyrus, left middle cingulate gyrus, left angular gyrus, right superior parietal gyrus and right middle frontal gyrus*(Table 2; Figure 1)*.

Table 2

The binarized gFCD differences between the SA and HC groups.

Brain areas	MNI coordinates			gFCD			
	X	Y	Z	BA	Peak voxels	Tvalue	ROI
HC>PAT							
Cerebellum_R	45	-75	-33		1350	4.25	Cluster 1
Temporal_Inf_R	48	-3	-39	20	99	3.87	Cluster 2
Lenticular_Nucleus,Putamen_L	-18	9	0		177	4.17	Cluster 3
Brain areas	MNI coordinates						
	X	Y	Z	BA	Peak voxels	Tvalue	ROI
HC<PAT							
Angular_Gyrus_R	45	-66	36	39	128	-4.02	Cluster 4
Angular_Gyrus_L	-42	-66	30	39	116	-3.45	Cluster 5
Cingulum_Mid_L	-9	-45	33	31	105	-3.77	Cluster 6
Frontal_Gyrus_Mid_R	42	27	39	8	41	-3.21	Cluster 7
Parietal_Gyrus_Sup_R	30	-54	66	7	47	-3.43	Cluster 8

Notes: Between-group differences in binarized gFCD at a threshold of r=0.3. Voxel-wise P<0.01 and cluster-level P<0.05 were used to identify significant group differences, correcting for multiple comparisons by AlphaSim.

Abbreviations: BA, Brodmann's area; gFCD, global functional connectivity density; MNI, Montreal Neurological Institute; SA, strabismus and amblyopia; PAT, patient; ROI, region of interest.

The lFCD values of children with SA were remarkably decreased in areas of the middle right temporal pole, right cerebellum, left lenticular nucleus, left putamen, bilateral hippocampus, left thalamus and left cerebellum; lFCD values were increased in the right superior parietal gyrus as compared with HC subjects *(Table 3; Figure 1)*

Table 3

The binarized lFCD differences between the SA and HC groups.

Brain areas	MNI coordinates			longFCD			
	X	Y	Z	BA	Peak voxels	Tvalue	ROI
HC>PAT							
Frontal_Inf_Tri_L	-45	12	24	44	31	4.14	Cluster 1
Precuneus_R	3	-72	45	7	50	3.43	Cluster 2
Cingulum_Ant_R	6	30	27	2	32	3.45	Cluster 3
Cingulum_Mid_R	6	-27	42	24	51	3.29	Cluster 4
Cingulum_Mid_L	-6	-3	42	24	43	4.01	Cluster 5
Supp_Motor_Area_L	-6	24	57	6	47	3.34	Cluster 6

Notes: Between-group differences in binarized lFCD at a threshold of r=0.3. Voxel-wise P<0.01 and cluster-level P<0.05 were used to identify significant group differences, correcting for multiple comparisons by AlphaSim.

Abbreviations: BA, Brodmann's area; lFCD, short-range functional connectivity density; MNI, Montreal Neurological Institute; SA, strabismus and amblyopia; PAT, patient.

2.3 ROC curve analysis

Based on findings of prior studies, we reasonably speculated that the difference between gFCD and lFCD values would be both statistically and clinically significant. Differences between gFCD and lFCD values may thus be considered to define an auxiliary diagnostic standard for highly probable. After consideration of accuracy and intuitiveness requirements for hypothesis verification, ROC analysis was performed. The area under the curve (AUC) value indicated the degree of accuracy; the greater the value, the higher the accuracy. An AUC value of 0.5-0.7 implied lower accuracy; a value of 0.7-0.9 implied average accuracy; a value of greater than 0.9 implied higher accuracy. The AUC values for gFCD were 0.787 for the right cerebellum; o.836 for the right temporal inferior region; 0.800 for the left lenticular nucleus and left putamen; 0.840 for the right angular gyrus; 0.741 for the left angular gyrus; 0.796 for the left cingulum mid; 0.775 for the right medial frontal gyrus; and 0.767 for the right superior parietal gyrus *(Figure 2).* The AUC values for lFCD were 0.787 for the right cerebellum; 0.800 for the middle right temporal pole; 0.760 for the left hippocampus; 0.792 for the left putamen; 0.881 for the right hippocampus, 0.881; 0.767 for the left thalamus; and 0.846 for the right superior frontal gyrus *(Figure 3).*

2.4 Correlation analyses

Patient anxiety score was found to be 7.23±2.33 while the depression score was found to be 7.63±1.20. Anxiety score was found to negatively correlate to right medial frontal gyrus voxel value (r=-0.845,

p<0.001); depression score was likewise find to negatively correlate with voxel value of that same region (r=-0.842, p<0.001).

3 Discussion

Compared with conventional fMRI, rs-fMRI does not require subjects to perform specific actions. This, in turn, allows for more accurate data collection. Compared with the HC subjects, changes in rs-fMRI and FCD results in children suffering SA suggest significant alterations in both patient brain activity and functional connections. Such abnormalities are of great relevance in relation to both the clinical manifestations and pathogenesis of SA and warrant detailed investigation. (Table 4)

Table 4
FCD method applied in ophthalmological diseases

Author	Year	Disease	Increase FCD	Decrease FCD
Chen et al [22]	2019	Primary Angle-closure Glaucoma	IFG PHG RMFG	CUN PoCG
Scheff et al [23]	2011	Alzheimer's disease	/	ITG
Myung et al [24]	2016	Adjustment disorder	/	MFG
Wang et al [25]	2014	Anisometropic Amblyopia	/	LIPL RPreCG LFFG LITG
Han et al [26]	2018	Neuromyelitis Optica	V1/V2	BA11 LING
Zhai et al [27]	2016	Pathological Myopia	/	PCG RPCG LFFG RSMG
Tan et al [28]	2016	Strabismus	/	MFG
Zhu, et al[21]	2019	corneal ulcer	MTG	MFG

The frontal lobe is widely involved in many physiological functions and its complexity far exceeds that of other central nervous system components. Anatomically, the precentral, superior frontal and inferior frontal sulci divide the frontal lobe into the precentral, superior frontal middle frontal and inferior frontal gyri. These regions all have distinct functions. Disorders of voluntary movement, language, and autonomic functions have been ascribed to frontal gyrus lesions. The frontal gyrus additionally plays a critical role in the maintenance of normal visual function. Previous studies reported SA patients to suffer abnormalities in frontal gyrus function. Patients suffering concomitant exotropia were found to have decreased left frontal gyrus volumes and decreased middle inferior gyrus gray matter density[21, 22]. The frontal eye field, located at the caudal end of the middle frontal gyrus, is vital in the control of eye movement and affects eye movement latency[23, 24]. In addition, earlier studies reported the frontal eye field to be pivotal in saccade formation [25, 26]. Xiao et al. found that children suffering amblyopia have

reduced gray matter density in the middle frontal gyrus[27]. Ouyang et al. similarly reported precentral gyrus gray matter volume to be reduced in such patients[28]. Furthermore, prefrontal cortex regional homogeneity and FCD were both found to be reduced in patients suffering anisometropic amblyopia[29]. In this study, as compared with HC subjects, gFCD values of SA patients were found to be decreased in the right superior frontal gyrus and increased in the right middle frontal gyrus (Fig. 4). Correlation analyses revealed that these phenomena influence patient anxiety and depression (Fig. 6).

The angular gyrus is located in the anterolateral parietal lobe and corresponds to Brodmann area 39. This region of the brain is crucial in sensory, visual, and auditory stimuli processing. Here, we found children suffering SA to have higher gFCD in the left and right angular gyrus as compared to HC subjects, likely due to compensatory increases in attention and spatial comprehension.

The thalamus is primarily responsible for relaying sensory and motor signals to the cerebral cortex[30]. Thalamic nuclei play fundamental roles in the relay of sensory information to the cerebral cortex. Notably, the thalamus is involved in the processing of visual information via the retino-thalamic-cortical pathway [31]. Studies have shown that abnormalities of this pathway affect pathogenesis of a number of neurological conditions, such as autism and temporal lobe epilepsy. Gray matter volume in the right thalamus was previously found to be increased in adults suffering strabismus[32]. In our study, SA patients were found to have decreased thalamic IFCD values, suggesting that thalamic involvement in the pathogenesis of SA is significant. The cingulate gyrus, a band of cortex surrounding the corpus callosum, is an integral component of the limbic system and the default mode network[33]. The cingulate gyrus establishes functional connections with the hippocampal cortex, medial prefrontal lobe, and temporal lobe cortex[34]. This brain region is closely involved executive functioning and emotional regulation. Prior studies have also focused on the role of cingulate gyrus in the pathogenesis and clinical manifestations of epilepsy[35, 36]. The anterior cingulate gyrus contains afferent thalamic projections[37]. Thus, this brain region likely plays an important role in eye movement and processing of visual information. In a study of patients suffering strabismus, Ouyang et al. observed that the gray matter volume of the right cingulate gyrus in strabismus patients was significantly reduced. On fMRI, the right cingulate gyrus was found to undergo significant activation in amblyopic patients who underwent perceptual learning therapy as compared to pre-treatment data, underscoring that dysfunction of this area plays an important role in the pathogenesis of amblyopia[38]. Here, gFCD values in the right middle cingulate gyrus of SA children were significantly increased as compared with HC subjects, consistent with findings reported previously. Recovery of cingulate gyrus function thus likely plays a compensatory role in treatment and can be considered as a component of future SA management.

The parahippocampal gyrus and hippocampus is involved in memory, recognition and spatial memory, also interconnecting with the visual system. The parahippocampal region is mainly responsible for memory formation in specific situations; the hippocampus is understood to play a role in long-term memory formation[39]. The anterior hippocampus is furthermore connected to the default mode network, ventral striatum, midbrain and amygdala; these areas play a role in the stress response. The posterior

hippocampus is more closely involved in spatial-contextual information processing. Studies have shown that damage to the hippocampus is associated with the development of Parkinson's disease[40]. When patients suffer from generalized anxiety disorder, their hippocampal volume significantly decreases[41]. McCormick found that the hippocampus and visual areas connect with each other throughout different phases of autobiographical memory formation[42]. In this study, the IFCD values were found to be decreased in the hippocampus bilaterally among SA patients as compared with HC subjects. These findings indicate that SA likely results in impairment of visual-spatial processing due to ocular dysfunction (Fig. 5) (Table 5)

Table 5
Brain regions with changed FCD values and its potential impact

Brain region	Brain function	Anticipated results
cerebellum	Regulating body balance and muscle tone; Coordinating of voluntary movement and language; emotion control; spatial cognition	The damage of spatial cognition
lenticular nucleus, putamen	Executive ability; language function.	Impairment of font-semantic pathway in visual pathway
superior frontal gyrus	Cognition; semantic system; episodic memory; indirectly control the sequences of visual-guided saccades and eye–hand coordination.	Reduced spatial cognitive ability; impairment of eye-hand coordination
angular gyrus	Visual language center	Compensatory enhancement of visual image and auditory image connection
middle cingulum gyrus	Executive ability; emotional management; visual function	Abnormality of visual function
superior parietal gyrus	Center of tactile and stereognosis	Stereognosis consumption increased
middle frontal gyrus	Consist of Frontal eye field	eye movements accuracy consumption increased
Temporal pole mid	Related to high-level social emotional function, implicated in theory of mind	Negative emotion, abnormal social function
Hippocampus	Long-term memory; associated with visual system; spatial information processing capability	The damage of spatial information processing capability
thalamus	involved in visual sensation; dynamic visual information management	The capability of dynamic visual information processing is impacted

4 Conclusion

Utilizing rs-fMRI as well as gFCD and lFCD values, we found abnormal neural activities in specific brain areas in children suffering SA. As our sample size was rather small, further research studying a larger patient population is warranted. Our findings lay the foundation for future clinical management of SA.

Declarations

Ethics approval

All research methods were approved by the committee of the medical ethics of the First Affiliated Hospital of Nanchang University and were in accordance with the 1964 Helsinki declaration and its later amendments or comparable ethical standards. Parents (or legal guardians) of all subjects were explained the purpose, methods, potential risks, and gave their consent to this study.

Consent to participate

All data generated or analyzed during this study from patients are included in this published article. All Patients and guardians were provided consent to publish these pictures.

Consent for publication

All authors have read and agreed to the published version of the manuscript.

Availability of data and material

Data used to support the findings of this study are available from the corresponding author upon request.

Competing interests

This was not an industry supported study. The authors report no conflicts of interest in this work.

Funding

This research is supported by National Natural Science Foundation of China (No: 81660158)

Authors' contributions

Conceptualization, Rong-Bin Liang And Qi Lin ;Methodology, Qian-Min Ge, Qi Lin; Formal analysis, Yi-Dan Shi, Rong-Bin Liang, Qian-Min Ge; Investigation, Biao Li, Wen-Qing Shi, Qi Lin, Qiu-Yu Li; Resources, Yi Shao; Data curation, Rong-Bin Liang , Yi-Dan Shi, Qian-Min Ge, Wen-Qing Shi, Qi Lin; Writing—original draft preparation, Yi-Dan Shi, Rong-Bin Liang; Writing—review and editing, Yi-Dan Shi, Qian-Min Ge, Yi Shao; Supervision, Yi Shao; Project administration, Yi Shao; Funding acquisition, Yi Shao.

Acknowledgements

Thanks Ophthalmology, The First Affiliated Hospital of Nanchang University, especially Dr. Yi Shao who helped us in this study.

References

1. LEWANDOWSKI K B. Strabismus as a possible sign of subclinical muscular dystrophy predisposing to rhabdomyolysis and myoglobinuria: a study of an affected family[J]. Can Anaesth Soc J, 1982, 29(4): 372–376.
2. DICKMANN A, PETRONI S, SALERNI A, et al. Effect of vertical transposition of the medial rectus muscle on primary position alignment in infantile esotropia with A- or V-pattern strabismus[J]. J AAPOS, 2011, 15(1): 14–16.
3. CHEN X, FU Z, YU J, et al. Prevalence of amblyopia and strabismus in Eastern China: results from screening of preschool children aged 36–72 months[J]. Br J Ophthalmol, 2016, 100(4): 515–519.
4. TARCZY-HORNOCH K, COTTER S A, BORCHERT M, et al. Prevalence and causes of visual impairment in Asian and non-Hispanic white preschool children: Multi-ethnic Pediatric Eye Disease Study[J]. Ophthalmology, 2013, 120(6): 1220–1226.
5. CHEN X, FU Z, YU J, et al. Prevalence of amblyopia and strabismus in Eastern China: results from screening of preschool children aged 36–72 months[J]. Br J Ophthalmol, 2016, 100(4): 515–519.
6. FU J, LI S M, LI S Y, et al. Prevalence, causes and associations of amblyopia in year 1 students in Central China: The Anyang childhood eye study (ACES)[J]. Graefes Arch Clin Exp Ophthalmol, 2014, 252(1): 137–143.
7. Prevalence of amblyopia and strabismus in African American and Hispanic children ages 6 to 72 months the multi-ethnic pediatric eye disease study[J]. Ophthalmology, 2008, 115(7): 1229–1236.
8. BEZ Y, COSKUN E, EROL K, et al. Adult strabismus and social phobia: a case-controlled study[J]. J AAPOS, 2009, 13(3): 249–252.
9. MOJON-AZZI S M, KUNZ A, MOJON D S. Strabismus and discrimination in children: are children with strabismus invited to fewer birthday parties?[J]. Br J Ophthalmol, 2011, 95(4): 473–476.
10. BROWN H D, WOODALL R L, KITCHING R E, et al. Using magnetic resonance imaging to assess visual deficits: a review[J]. Ophthalmic Physiol Opt, 2016, 36(3): 240–265.

11. HUANG X, ZHONG Y L, ZENG X J, et al. Disturbed spontaneous brain activity pattern in patients with primary angle-closure glaucoma using amplitude of low-frequency fluctuation: a fMRI study[J]. Neuropsychiatr Dis Treat, 2015, 11: 1877–1883.
12. ZHU F, TANG L, ZHU P, et al. Resting-state functional magnetic resonance imaging (fMRI) and functional connectivity density mapping in patients with corneal ulcer[J]. Neuropsychiatr Dis Treat, 2019, 15: 1833–1844.
13. TOMASI D, VOLKOW N D. Functional connectivity density mapping[J]. Proc Natl Acad Sci U S A, 2010, 107(21): 9885–9890.
14. ZUO X N, EHMKE R, MENNES M, et al. Network centrality in the human functional connectome[J]. Cereb Cortex, 2012, 22(8): 1862–1875.
15. ZHANG J, BI W, ZHANG Y, et al. Abnormal functional connectivity density in Parkinson's disease[J]. Behav Brain Res, 2015, 280: 113–118.
16. HATA M, KAZUI H, TANAKA T, et al. Functional connectivity assessed by resting state EEG correlates with cognitive decline of Alzheimer's disease - An eLORETA study[J]. Clin Neurophysiol, 2016, 127(2): 1269–1278.
17. MAGLANOC L A, LANDRO N I, JONASSEN R, et al. Data-Driven Clustering Reveals a Link Between Symptoms and Functional Brain Connectivity in Depression[J]. Biol Psychiatry Cogn Neurosci Neuroimaging, 2019, 4(1): 16–26.
18. LI Q, JIANG Q, GUO M, et al. Grey and white matter changes in children with monocular amblyopia: voxel-based morphometry and diffusion tensor imaging study[J]. Br J Ophthalmol, 2013, 97(4): 524–529.
19. LIANG M, XIE B, YANG H, et al. Altered interhemispheric functional connectivity in patients with anisometropic and strabismic amblyopia: a resting-state fMRI study[J]. Neuroradiology, 2017, 59(5): 517–524.
20. CARLSON M E, SILVA H S, CONBOY I M. Aging of signal transduction pathways, and pathology[J]. Exp Cell Res, 2008, 314(9): 1951–1961.
21. YAN X, LIN X, WANG Q, et al. Dorsal visual pathway changes in patients with comitant extropia[J]. PLoS One, 2010, 5(6): e10931.
22. XIAO J X, XIE S, YE J T, et al. Detection of abnormal visual cortex in children with amblyopia by voxel-based morphometry[J]. Am J Ophthalmol, 2007, 143(3): 489–493.
23. BLANKE O, SPINELLI L, THUT G, et al. Location of the human frontal eye field as defined by electrical cortical stimulation: anatomical, functional and electrophysiological characteristics[J]. Neuroreport, 2000, 11(9): 1907–1913.
24. VERNET M, QUENTIN R, CHANES L, et al. Frontal eye field, where art thou? Anatomy, function, and non-invasive manipulation of frontal regions involved in eye movements and associated cognitive operations[J]. Front Integr Neurosci, 2014, 8: 66.
25. FERNANDES H L, STEVENSON I H, PHILLIPS A N, et al. Saliency and saccade encoding in the frontal eye field during natural scene search[J]. Cereb Cortex, 2014, 24(12): 3232–3245.

26. TEHOVNIK E J, SOMMER M A, CHOU I H, et al. Eye fields in the frontal lobes of primates[J]. Brain Res Brain Res Rev, 2000, 32(2–3): 413–448.
27. XIAO J X, XIE S, YE J T, et al. Detection of abnormal visual cortex in children with amblyopia by voxel-based morphometry[J]. Am J Ophthalmol, 2007, 143(3): 489–493.
28. OUYANG J, YANG L, HUANG X, et al. The atrophy of white and gray matter volume in patients with comitant strabismus: Evidence from a voxel-based morphometry study[J]. Mol Med Rep, 2017, 16(3): 3276–3282.
29. LIN X, DING K, LIU Y, et al. Altered spontaneous activity in anisometropic amblyopia subjects: revealed by resting-state FMRI[J]. PLoS One, 2012, 7(8): e43373.
30. BASSO M A, UHLRICH D, BICKFORD M E. Cortical function: a view from the thalamus[J]. Neuron, 2005, 45(4): 485–488.
31. MARTIN P R. Colour through the thalamus[J]. Clin Exp Optom, 2004, 87(4–5): 249–257.
32. CHAN S T, TANG K W, LAM K C, et al. Neuroanatomy of adult strabismus: a voxel-based morphometric analysis of magnetic resonance structural scans[J]. Neuroimage, 2004, 22(2): 986–994.
33. SAN P E, MOUNTZ J M, OJHA B, et al. Anterior cingulate gyrus epilepsy: the role of ictal rCBF SPECT in seizure localization[J]. Epilepsia, 2000, 41(5): 594–600.
34. OSTOJIC J, KOZIC D, PAVLOVIC A, et al. Hippocampal diffusion tensor imaging microstructural changes in vascular dementia[J]. Acta Neurol Belg, 2015, 115(4): 557–562.
35. BRAGA A M, FUJISAO E K, VERDADE R C, et al. Investigation of the cingulate cortex in idiopathic generalized epilepsy[J]. Epilepsia, 2015, 56(11): 1803–1811.
36. ALKAWADRI R, SO N K, Van NESS P C, et al. Cingulate epilepsy: report of 3 electroclinical subtypes with surgical outcomes[J]. JAMA Neurol, 2013, 70(8): 995–1002.
37. UNNWONGSE K, WEHNER T, FOLDVARY-SCHAEFER N. Mesial frontal lobe epilepsy[J]. J Clin Neurophysiol, 2012, 29(5): 371–378.
38. ZHAI J, CHEN M, LIU L, et al. Perceptual learning treatment in patients with anisometropic amblyopia: a neuroimaging study[J]. Br J Ophthalmol, 2013, 97(11): 1420–1424.
39. PARRA M A, CALIA C, GARCIA A F, et al. Refining memory assessment of elderly people with cognitive impairment: Insights from the short-term memory binding test[J]. Arch Gerontol Geriatr, 2019, 83: 114–120.
40. DUBOIS B, HAMPEL H, FELDMAN H H, et al. Preclinical Alzheimer's disease: Definition, natural history, and diagnostic criteria[J]. Alzheimers Dement, 2016, 12(3): 292–323.
41. ABDALLAH C G, COPLAN J D, JACKOWSKI A, et al. A pilot study of hippocampal volume and N-acetylaspartate (NAA) as response biomarkers in riluzole-treated patients with GAD[J]. Eur Neuropsychopharmacol, 2013, 23(4): 276–284.
42. MCCORMICK C, ST-LAURENT M, TY A, et al. Functional and effective hippocampal-neocortical connectivity during construction and elaboration of autobiographical memory retrieval[J]. Cereb

Cortex, 2015, 25(5): 1297–1305.

Figures

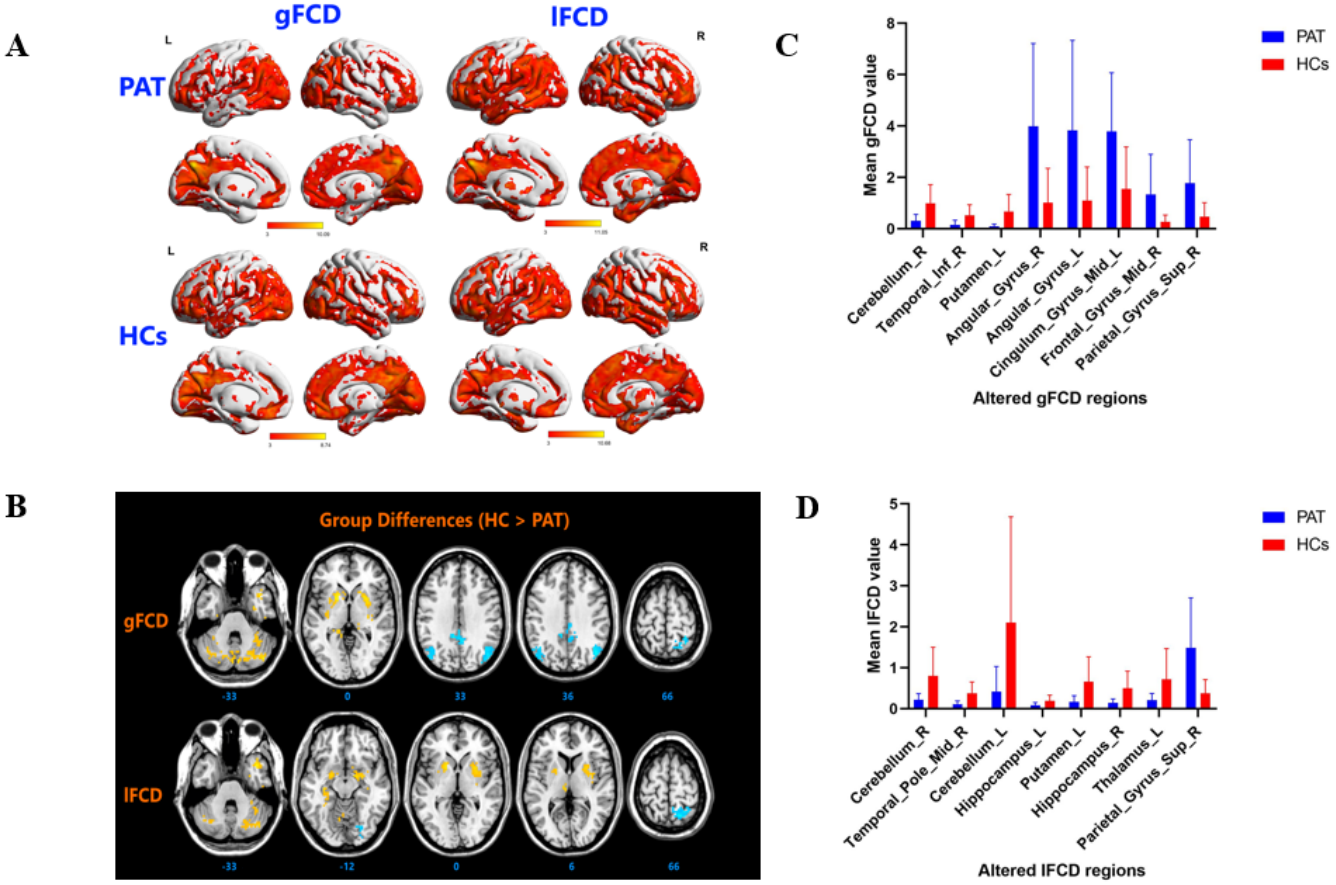

Figure 1

(A)Binarized gFCD (left) and lFCD (right) values in different brain regions. Red and blue bars indicate the HC and SA groups, respectively. (B)The red areas depict higher gFCD and lFCD values. Significant gFCD differences were observed in the right cerebellum, left lenticular nucleus, left putamen and right superior frontal gyrus, right angular gyrus, left middle cingulate gyrus, left angular gyrus, right superior parietal gyrus and right middle frontal gyrus. The color bars show the means of altered longFCD between the SA and HC groups. Significant lFCD differences were observed in the middle right temporal pole, right cerebellum, left lenticular nucleus, left putamen, bilateral hippocampus, left thalamus and left cerebellum, right superior parietal gyrus. The color bars show the means of altered lFCD between the SA group and HCs. (C) Binarized gFCD and lFCD differences between the HC and SA groups. Yellow areas show lower values. Abbreviations: gFCD, global functional connectivity density; lFCD, short-range functional connectivity density; PAT, patient; HCs, healthy controls; L, left; R, right.

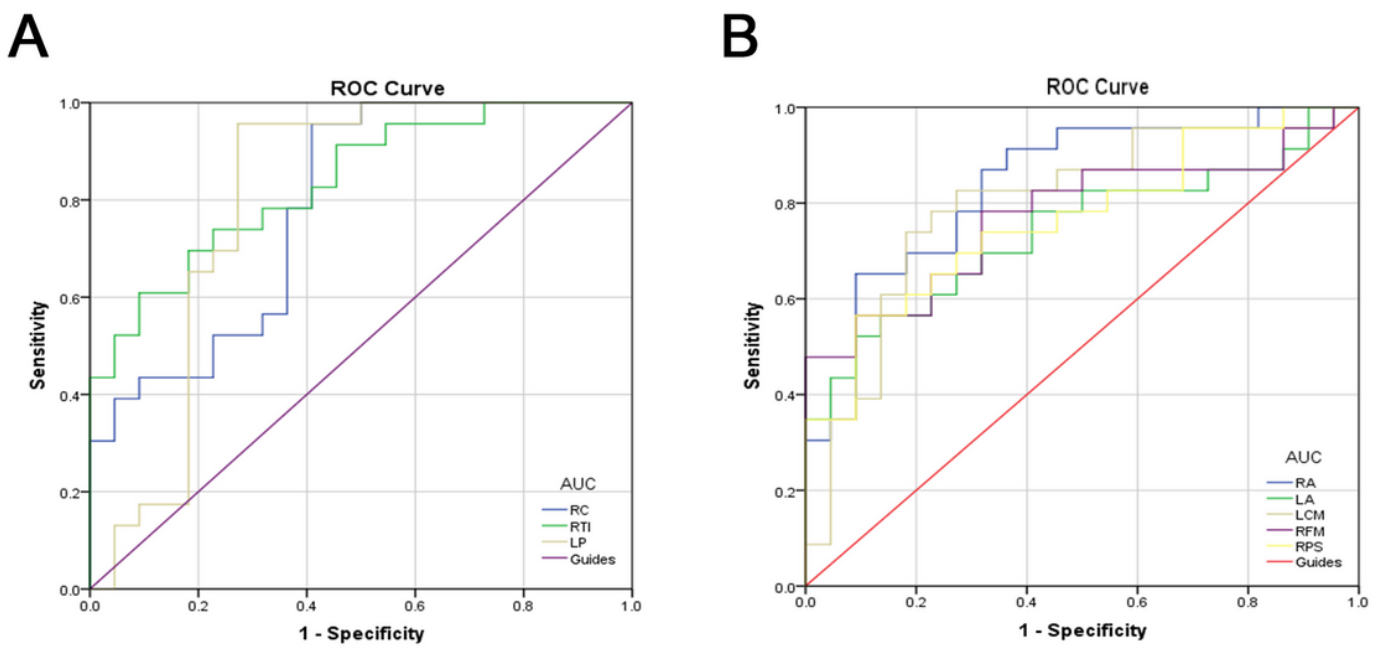

Figure 2

ROC curve analysis of the mean gFCD difference for altered brain regions. (A) The area under the ROC curve were 0.787, (p = 0.001; 95% CI: 0.653-0.920) for RC, RTI 0.836, (p□0.0001; 95% CI: 0.722-0.950), LP 0.800, (p = 0.001; 95% CI: 0.654-0.947). (B) The area under the ROC curve were 0.840, (p□0.0001; 95% CI: 0.723-0.956) for RA, LA 0.741, (p = 0.006; 95% CI: 0.593-0.889), LCM 0.796, (p = 0.001; 95% CI: 0.661-0.932), RFM 0.775, (p = 0.002; 95% CI: 0.634-0.915), RPS 0.767, (p = 0.002; 95% CI: 0.628-0.905). Abbreviations: AUC, area under the curve; ROC, receiver operating characteristic. RC, right cerebellum; RTI, right temporal inf; LP, left putamen; RA, right angular; LA, left angular; LCM, left cingulum mid; RFM, right frontal mid; RPS, right parietal sup.

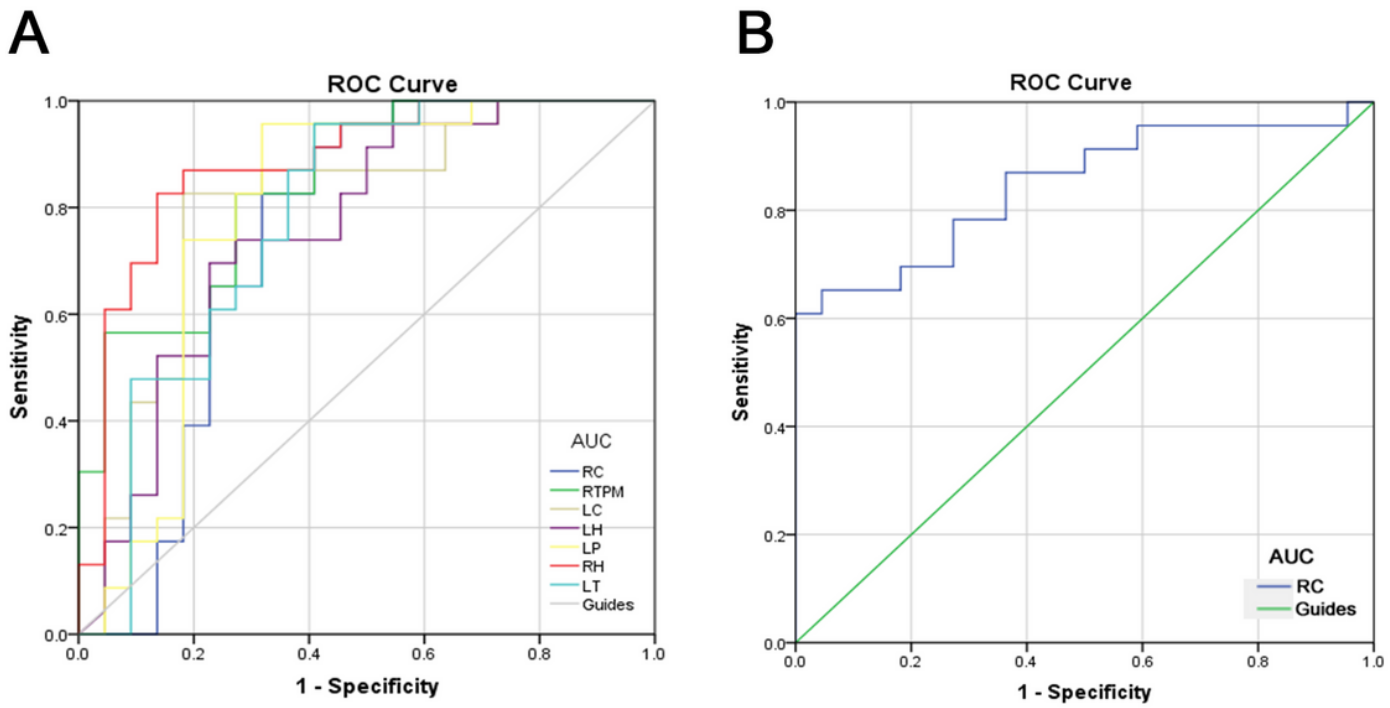

Figure 3

ROC curve analysis of the mean IFCD difference for altered brain regions. (A) The area under the ROC curve were 0.787, (p = 0.005; 95% CI: 0.583-0.903) for RC, right cerebellum; RTPM, right temporal pole mid; LC, left cerebellum; LH, left hippocampus; LP, left putamen; RH, right hippocampus; LT, left thalamus; RPS, right parietal sup. Abbreviations: AUC, area under the curve; ROC, receiver operating characteristic. RC, right cerebellum; RTPM, LC 0.800, (p = 0.001; 95% CI: 0.663-0.938) , LH 0.760, (p = 0.003; 95% CI: 0.616-0.904), LP 0.792, (p = 0.001; 95% CI: 0.645-0.940), RH 0.881, (p = 0.053; 95% CI: 0.778-0.985), LT 0.767, (p = 0.073; 95% CI: 0.635-0.922). (B) The area under the ROC curve were 0.846, (p□0.0001; 95% CI: 0.730-0.962) for RPS.

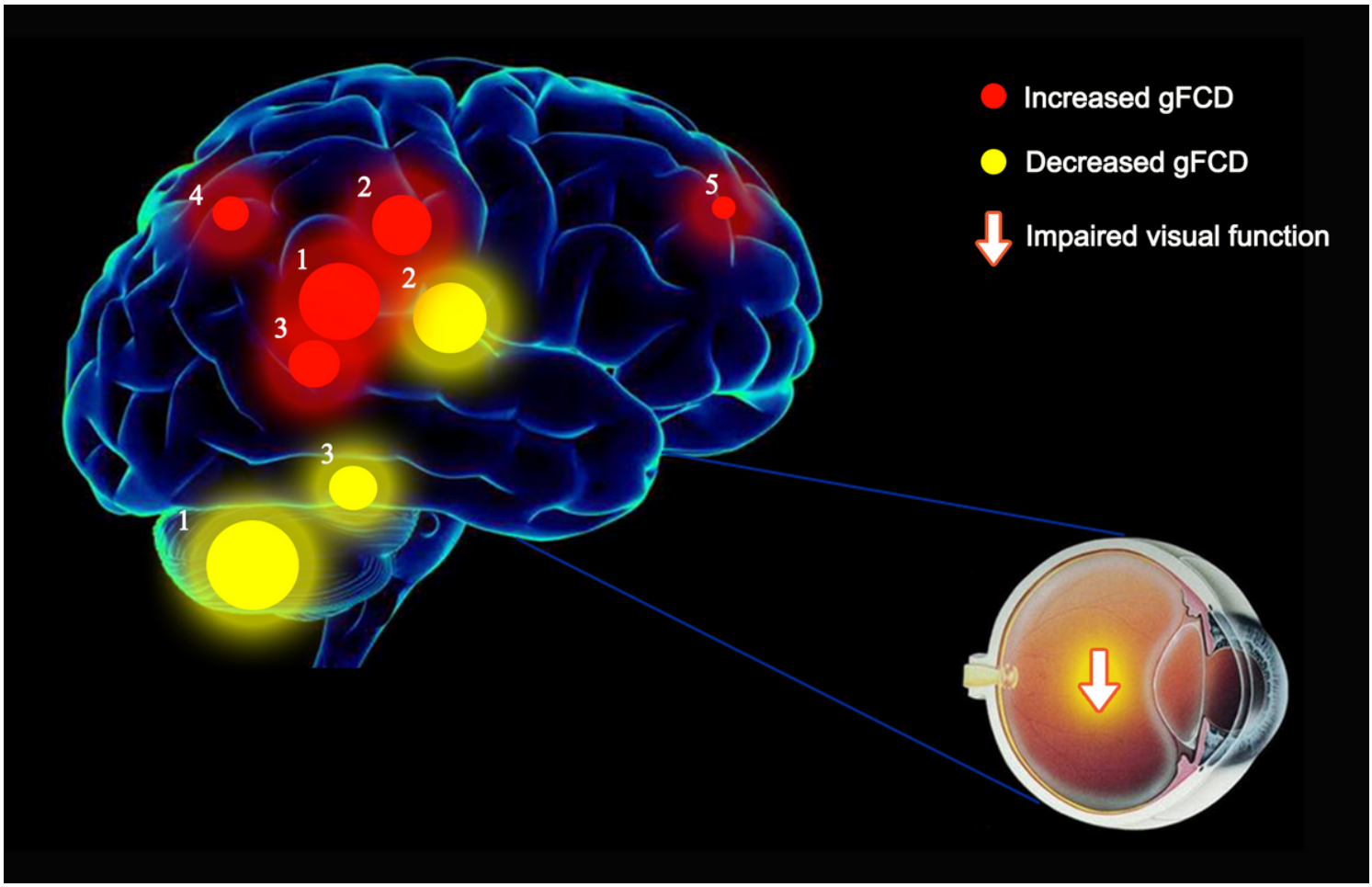

Figure 4

The mean gFCD values of altered brain regions. Compared with the HCs, the gFCD values of the following regions were decreased to various extents: 1- Right cerebellum (t = 4.25), 2- Left putamen (t = 4.17), 3- Right frontal sup (BA 10, t = -4.27). Compared with the HCs, the gFCD values of the following regions were increased to various extents: 1- Right angular (BA 39, t = -4.02), 2- Left cingulum mid (BA 31, t = -3.77), 3- Left angular (BA 39, t = -3.45), 4- Right parietal sup (BA 7, t = -3.43), 5- Right frontal mid (BA 8, t = -3.21). Abbreviations: HCs, healthy controls; BA, Brodmann's area.

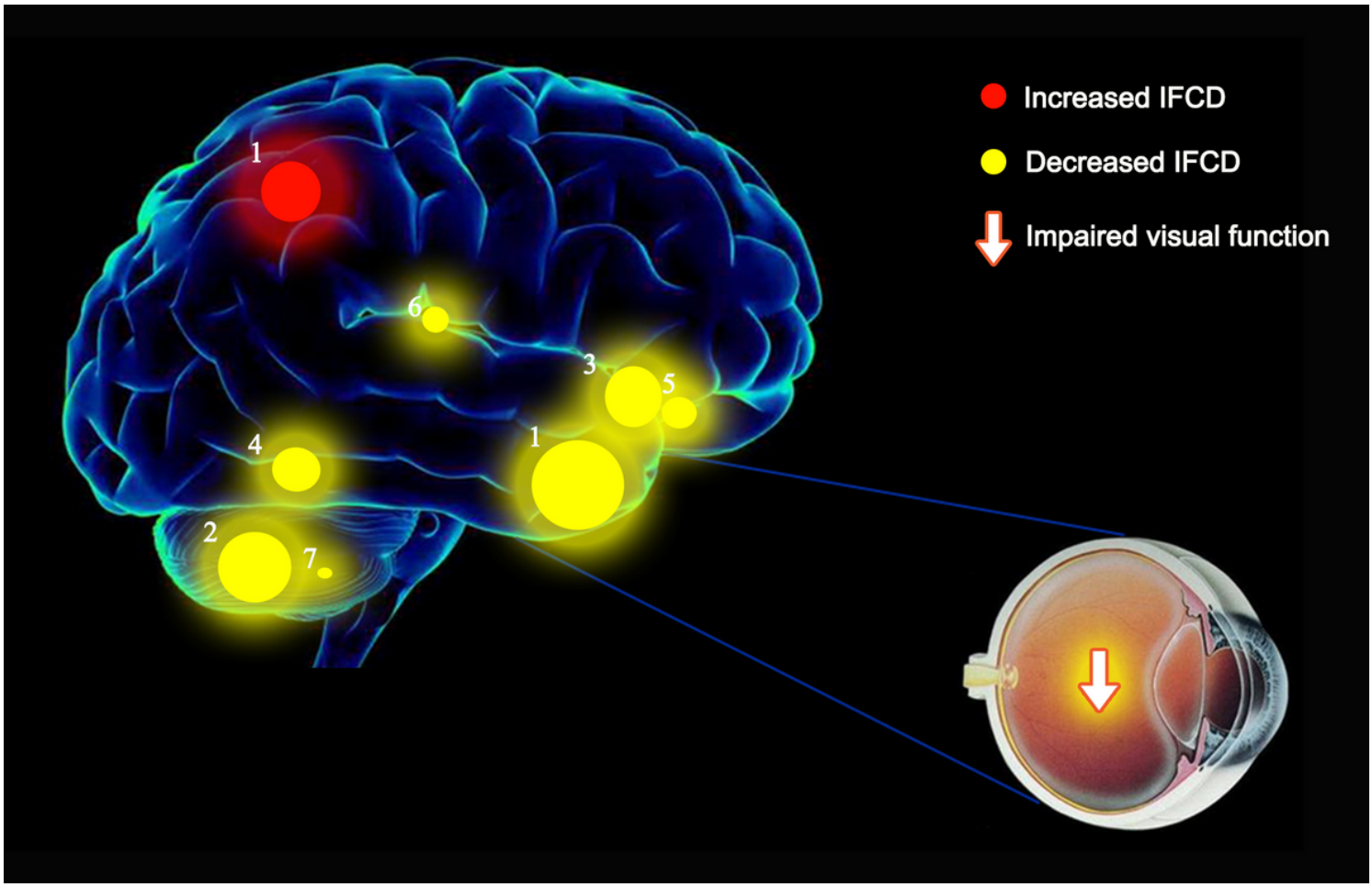

Figure 5

The mean IFCD values of altered brain regions. Compared with the HCs, the IFCD values of the following regions were decreased to various extents: 1- Right temporal pole mid (BA 38, t = 4.50), 2- Right cerebellum (t = 3.90), 3- Left putamen (BA 34, t = 3.80), 4- Left hippocampus (BA 37, t = 3.43), 5- Right hippocampus (BA 34, t = 4.00), 6- Left thalamus (t = 3.20), 7- Left cerebellum (t = 3.08). Compared with the HCs, the IFCD values of the following regions were increased to various extents: 1- Right parietal sup (BA 7, t = -4.1). Abbreviations: HCs, healthy controls; BA, Brodmann's area.

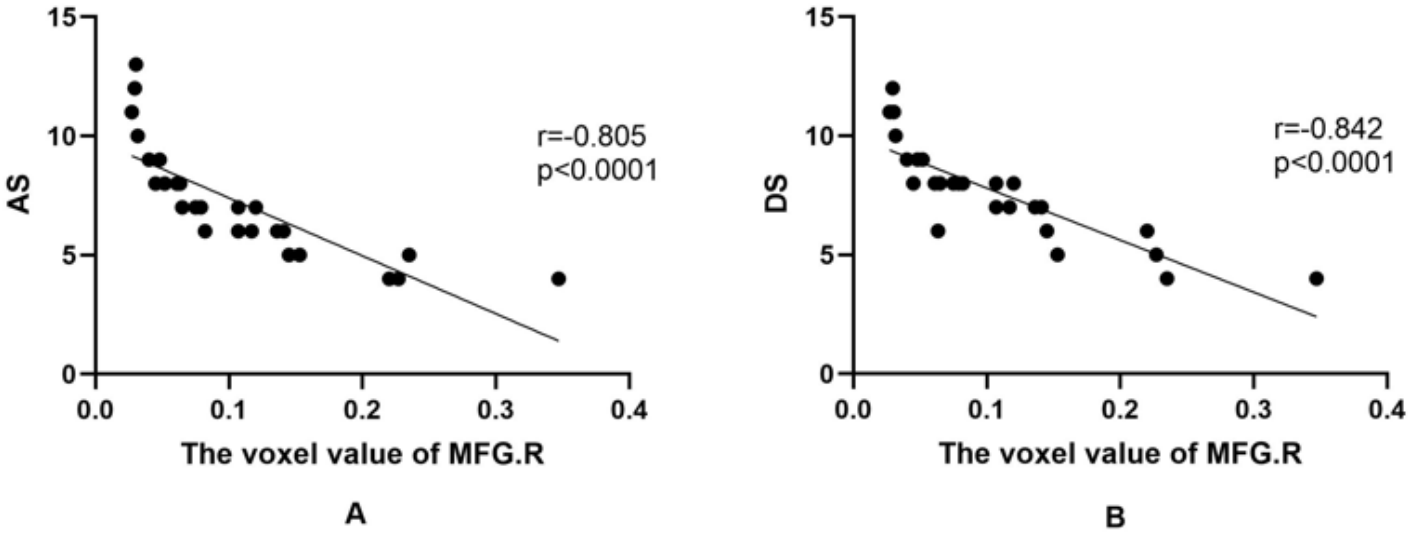

Figure 6

Correlations between the voxel value of right media frontal gyrus and clinical behaviors. (a) The AS showed a negative correlation with the voxel values of right medial frontal gyrus (r=-0.845, p<0.001), and (b) the DS showed a negative correlation with the voxel values of right medial frontal gyrus (r=-0.842, p<0.001) Abbreviations: MFG.R, right media frontal gyrus; AS, anxiety scores; DS, depression scores.